Agreement of Anterior Segment Parameters Obtained From Swept-Source Fourier-Domain and Time-Domain Anterior Segment Optical Coherence Tomography

Sunee Chansangpetch,[1,2] Anwell Nguyen,[1] Marta Mora,[1] Mai Badr,[1] Mingguang He,[3,4] Travis C. Porco,[1] and Shan C. Lin[1]

[1]Department of Ophthalmology, University of California, San Francisco, California, United States
[2]Department of Ophthalmology, Chulalongkorn University and King Chulalongkorn Memorial Hospital, Thai Red Cross Society, Bangkok, Thailand
[3]State Key Laboratory of Ophthalmology, Zhongshan Ophthalmic Center, Sun Yat-sen University, Guangzhou, China
[4]Centre of Eye Research Australia, University of Melbourne, Royal Victorian Eye and Ear Hospital, East Melbourne, Australia

PURPOSE. To assess the interdevice agreement between swept-source Fourier-domain and time-domain anterior segment optical coherence tomography (AS-OCT).

METHODS. Fifty-three eyes from 41 subjects underwent CASIA2 and Visante OCT imaging. One hundred eighty–degree axis images were measured with the built-in two-dimensional analysis software for the swept-source Fourier-domain AS-OCT (CASIA2) and a customized program for the time-domain AS-OCT (Visante OCT). In both devices, we examined the angle opening distance (AOD), trabecular iris space area (TISA), angle recess area (ARA), anterior chamber depth (ACD), anterior chamber width (ACW), and lens vault (LV). Bland-Altman plots and intraclass correlation (ICC) were performed. Orthogonal linear regression assessed any proportional bias.

RESULTS. ICC showed strong correlation for LV (0.925) and ACD (0.992) and moderate agreement for ACW (0.801). ICC suggested good agreement for all angle parameters (0.771–0.878) except temporal AOD500 (0.743) and ARA750 (nasal 0.481; temporal 0.481). There was a proportional bias in nasal ARA750 (slope 2.44, 95% confidence interval [CI]: 1.95–3.18), temporal ARA750 (slope 2.57, 95% CI: 2.04–3.40), and nasal TISA500 (slope 1.30, 95% CI: 1.12–1.54). Bland-Altman plots demonstrated in all measured parameters a minimal mean difference between the two devices (−0.089 to 0.063); however, evidence of constant bias was found in nasal AOD250, nasal AOD500, nasal AOD750, nasal ARA750, temporal AOD500, temporal AOD750, temporal ARA750, and ACD. Among the parameters with constant biases, CASIA2 tends to give the larger numbers.

CONCLUSIONS. Both devices had generally good agreement. However, there were proportional and constant biases in most angle parameters. Thus, it is not recommended that values be used interchangeably.

Keywords: CASIA2, Visante OCT, anterior segment optical coherence tomography, swept-source Fourier-domain anterior segment optical coherence tomography, time-domain anterior segment optical coherence tomography

G laucoma is the leading cause of irreversible blindness worldwide.[1] Angle closure glaucoma (ACG) is a major form of glaucoma that is characterized by narrowing of the anterior chamber angle, usually with the presence of iridotrabecular contact. ACG creates greater morbidity than open angle glaucoma and accounts for approximately 50% of bilateral glaucoma blindness.[2,3]

Due to the difference in management strategy, it is important to discern the ACG from the open angle type. Currently, optical coherence tomography (OCT) has an increasing role in the evaluation of the anterior segment as an adjunct to standard gonioscopy examination. Anterior segment OCT (AS-OCT) can provide both qualitative and quantitative information that is beneficial for the assessment for narrow/closed angles.

Since the introduction of the first-generation time-domain (TD) AS-OCT (Visante OCT), there have been numerous publications using this machine to assess various aspects of angle structure and anterior segment anatomy.[4,5] Several parameters obtained by the Visante OCT have been shown to have excellent diagnostic ability for angle closure disease.[6-10]

Recently, the latest swept-source Fourier-domain AS-OCT, CASIA2, has been introduced, which provides faster scanning speed and higher resolution.[11] The device also has built-in software that allows automated and/or manual measurement of various parameters.

Although both Visante OCT and CASIA2 are specifically designed for anterior segment scanning, there are some dissimilarities due to the differences in scanning speed, image resolution and postimaging measurement process. There has
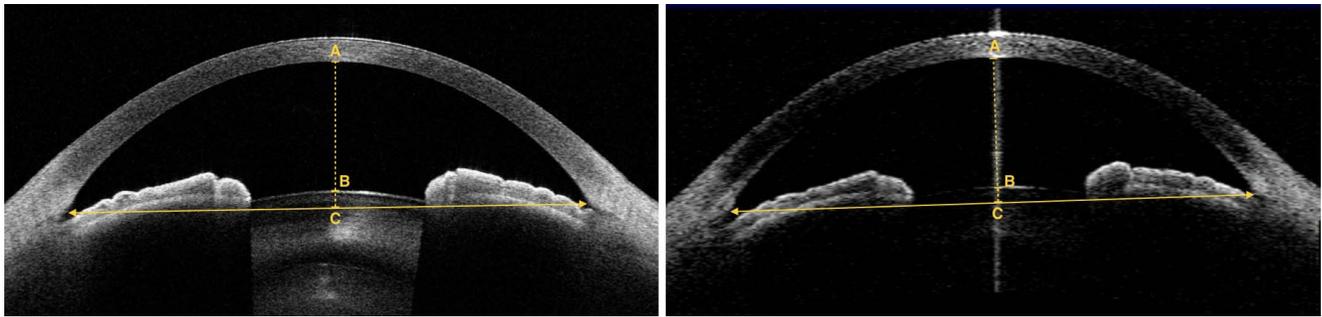
FIGURE 1. Example images obtained at 180-degree axis of the same eye. (*Left*) CASIA2 image and (*right*) Visante OCT image. *Arrowheads* indicate location of scleral spurs; *line* with *arrowheads* indicates scleral spur–to–scleral spur distance or anterior chamber width (ACW); *dashed line* indicates a perpendicular bisector of ACW line, which intersects with corneal endothelium (**A**), anterior lens surface (**B**), and ACW line (**C**). The length of AB represents anterior chamber depth (ACD), and BC represents lens vault (LV).

been speculation as to whether values obtained from CASIA2 are equivalent to those from Visante OCT. We aimed to assess the interdevice agreement of the anterior segment parameters obtained from these two AS-OCT devices to answer whether their values were interchangeable and what the offset between the devices were, if any.

METHODS

Institutional review board approval was obtained from the University of California, San Francisco. This study was conducted in accordance with the tenets of the Declaration of Helsinki. The subjects were enrolled between September 2016 and June 2017. Written informed consent was obtained for all individuals before enrollment in this study.

Subjects

The subjects were recruited from general ophthalmology and glaucoma clinics at the University of California, San Francisco. The inclusion criteria were age greater than 20 years old and no history of any intraocular surgery or laser. Exclusion criteria included any corneal or conjunctival abnormalities precluding adequate assessment of the anterior chamber by AS-OCT, active ocular infection, or inability to perform the test.

All subjects underwent slit-lamp examination, Goldmann applanation tonometry, and gonioscopy by a single examiner (SCL). Eyes that had Shaffer angle grading 1 or less for 180 degrees or more were defined as closed angle; otherwise, they were considered to be open angle.

All subjects were scanned with both Visante OCT and CASIA2 after 5 minutes of dark adaptation (<1 lux illumination at the imaging plane). Scans were performed by a single trained operator. An assistant helped in holding the subjects' eyelids, which was done gently to avoid pressure to the globe, in the same manner for both devices. The sequence of the devices was randomized to prevent time- or illumination-dependent differences in ocular anatomy.

Visante OCT Image Acquisition

Visante OCT (software version 3.0.1.8; Carl Zeiss Meditec, Inc., Dublin, CA, USA) images were acquired using the anterior segment single mode. The alignment of the scanning line was adjusted to go through the center of the pupil, with temporal and nasal angles aligned on the 180-degree axis. The image quality was assessed by the operator during the acquisition. The images that showed the interference beam along the visual axis indicating proper eye alignment and had the best quality

in terms of the visualization of the scleral spurs and ARAs were chosen and exported for further analysis.

CASIA2 Image Acquisition

The angle analysis mode, which is comprised of 16 consecutive meridional scans (800 A-scans per line), was used for CASIA2 (Tomey Corporation, Nagoya, Japan) image acquisition. The scan was performed using the autoalignment function. The image quality was assessed during the acquisition by the operator. Only the images from the horizontal (180-degree) alignment were used for the analysis. The horizontal images that had poor visualization of the scleral spurs and angle areas were excluded. Example images from Visante OCT and CASIA2 are shown in Figure 1.

Image Analysis

One best-quality image per subject from each device was used for analysis. All images were analyzed by a fellowship-trained grader (SC) who was masked to the clinical and gonioscopic results. The grading for Visante OCT and CASIA2 was done separately, and the image sequence was in a random fashion.

For the images from Visante OCT, the measurements were performed using a customized software, the Zhongshan Angle Assessment Program (ZAAP; Guangzhou, China), which automatically calculated the parameters after manual identification of the temporal and nasal scleral spurs (SS). The CASIA2 images were analyzed by a built-in 2D Analysis software that automatically calculated the measurements along with the structural outlines and reference lines. Although the software automatically generates the SS marks, the grader rechecked and manually adjusted the position of the SS where appropriate to assure that the grading was done in the same way as with Visante OCT. For both devices, the software-generated image outlines and reference lines were assessed by the grader to assure the accuracy of the measurements. The outline tracer was edited where needed in CASIA2. However, in Visante OCT, the customized software does not allow for manually adjusting the outline tracers. Thus, the eyes for which the Visante images had incorrect ZAAP software-generated outlines were excluded.

The determination of SS was based on (1) the point at which there was a change in curvature in the corneoscleral-aqueous interface,[12] (2) the apex of an internal projection of the inner margin of the cornea and trabecular meshwork, and (3) the point at which the interface line between the less-reflective ciliary muscle and sclera intersects with the inner corneal margin.[13]

TABLE. Comparison of Anterior Segment Parameters on AS-OCT as Measured by CASIA2 and Visante OCT

	CASIA2		Visante OCT				Mean Difference	95% CI of Mean Difference	LOA
	Mean	SD	Mean	SD	ICC	95% CI of ICC			
Nasal angle parameters									
AOD250, mm	0.198	0.103	0.169	0.127	0.790	0.663 to 0.873	0.029	0.010 to 0.048	−0.111 to 0.169
AOD500, mm	0.251	0.131	0.216	0.145	0.823	0.713 to 0.894	0.035	0.014 to 0.056	−0.117 to 0.187
AOD750, mm	0.348	0.175	0.292	0.184	0.838	0.736 to 0.903	0.055	0.031 to 0.080	−0.121 to 0.232
ARA750, mm^2	0.190	0.095	0.279	0.193	0.481	0.246 to 0.663	−0.089	−0.127 to −0.052	−0.361 to 0.182
TISA500, mm^2	0.103	0.050	0.105	0.063	0.850	0.754 to 0.910	−0.001	−0.010 to 0.007	−0.064 to 0.061
TISA750, mm^2	0.179	0.084	0.173	0.101	0.878	0.798 to 0.928	0.007	−0.006 to 0.019	−0.085 to 0.099
Temporal angle parameters									
AOD250, mm	0.185	0.102	0.166	0.112	0.820	0.707 to 0.892	0.015	−0.002 to 0.032	−0.110 to 0.140
AOD500, mm	0.240	0.141	0.204	0.135	0.743	0.594 to 0.843	0.036	0.011 to 0.062	−0.151 to 0.224
AOD750, mm	0.324	0.175	0.261	0.161	0.774	0.640 to 0.863	0.063	0.036 to 0.090	−0.130 to 0.257
ARA750, mm^2	0.175	0.095	0.257	0.200	0.481	0.246 to 0.663	−0.083	−0.122 to −0.043	−0.370 to 0.204
TISA500, mm^2	0.096	0.050	0.099	0.056	0.771	0.634 to 0.861	−0.003	−0.013 to 0.007	−0.075 to 0.069
TISA750, mm^2	0.167	0.087	0.170	0.092	0.809	0.691 to 0.885	0.004	−0.010 to 0.019	−0.103 to 0.112
Anterior chamber and lens parameters									
ACD, mm	2.477	0.332	2.459	0.333	0.992	0.987 to 0.996	0.018	0.008 to 0.028	−0.057 to 0.093
ACW, mm	11.687	0.388	11.754	0.432	0.801	0.679 to 0.880	−0.067	−0.136 to 0.003	−0.573 to 0.440
LV, mm	0.599	0.301	0.608	0.316	0.925	0.873 to 0.956	−0.009	−0.043 to 0.024	−0.250 to 0.232

CI, confidence interval; LOA, limits of agreement.

From the analysis software used in this study, six angle parameters, two anterior chamber parameters, and one lens parameter were available for comparison between the two machines. Iris parameters were not included in the study because they are not available in the 2D Analysis setting of the CASIA2 machine. The angle parameters included angle opening distance (AOD) at 250, 500, and 750 μm from the SS (AOD250, AOD500, and AOD750); angle recess area (ARA) at 750 μm from the SS (ARA750); and trabecular iris space area (TISA) at 500 and 750 μm from the SS (TISA500 and TISA750). The anterior chamber parameters included anterior chamber depth (ACD) and anterior chamber width (ACW). The lens parameter was lens vault (LV). The definitions of each parameter have been previously described.[14] The comparison of each angle parameter was done separately for the nasal and temporal angles.

Statistical Analysis

Means and standard deviations were calculated for continuous variables. The data were shown as counts and percentages for categorical variables. Intraclass correlation coefficients (ICC) for absolute agreement[15] and Bland-Altman plots were used to assess the agreement between parameters from the two devices. In addition to the Bland-Altman plots, we reported the bootstraps percentile interval (2.5th to 97.5th percentile [P2.5 to P95.7]) for the estimated regression of slope to assess the relationship of the difference as the function of the mean. Orthogonal linear regression was performed to assess for any proportional bias and constant offset. All analyses were performed using R version 3.3 for Macintosh (R Foundation for Statistical Computing, Vienna, Austria).

RESULTS

A total of seven eyes from seven subjects were initially excluded from the study due to poor image quality. All the exclusions were Visante OCT images, including two images in which the SS could not be clearly identified, four images that had poor quality at the apex of the angle, and three eyes with incorrect image outlines by the ZAAP software.

After image exclusion, the study was comprised of 53 eyes from 41 subjects. The mean (SD) age of the subjects was 70.9 (8.4) years, ranging from 52 to 86 years old. Of 41 subjects, 29 (70.7%) were females and 12 (29.3%) were males. Of the 53 studied eyes, the mean (SD) visual acuity in decimals was 0.82 (0.22). Regarding the angle status as classified by gonioscopy, 32 (60.4%) eyes were in the open group and 21 (39.6%) eyes were in the closed group. The characteristics of anterior segment parameters obtained from CASIA2 and Visante AS-OCT, as well as the analysis of the interdevice agreement, are shown in the Table.

The ICC for LV showed excellent correlation (0.925). The ICCs for angle parameters suggested good agreement (up to 0.878) except for temporal AOD500 and ARA750. For temporal AOD500, we found moderate agreement (ICC 0.743), while for ARA750, we found poor agreement (nasal ARA750: ICC 0.481; temporal ARA750: ICC 0.481). For anterior chamber parameters, ICC showed evidence of excellent agreement for ACD (0.992) and moderate agreement for ACW (0.801).[15]

Bland-Altman plots showed good agreement in all parameters with narrow limits of agreement (LOA) (Figs. 2–4). All measured parameters demonstrated minimal mean difference between the two devices (−0.089 to 0.0263). Examining the Bland-Altman plots, we found evidence that the line of equity (mean difference of zero) resided outside the 95% confidence interval (CI) of the mean difference for the following: nasal AOD250, nasal AOD500, nasal AOD750, nasal ARA750, temporal AOD500, temporal AOD750, temporal ARA750, and ACD. In addition, The bootstraps percentile interval for the estimated regression of slope showed that the variability of the differences between the devices was significantly dependent on the magnitude of the measurements for nasal ARA750 (P2.5 to P95.7: −0.990 to −0.582); temporal ARA750 (P2.5 to P95.7: −1.076 to −0.665); nasal TISA500 (P2.5 to P95.7: −0.413 to −0.116); and nasal TISA750 (P2.5 to P95.7: −0.335 to −0.067). Among parameters that possessed significant biases, CASIA2 tended to provide higher measurements in most angle parameters and ACD, while the ARA750 values from the Visante OCT tended to be higher than those from the CASIA2.

The orthogonal regression evidence of proportional bias existed for nasal ARA750 (slope 2.44, 95% CI 1.95–3.18), temporal ARA750 (slope 2.57, 95% CI: 2.04–3.40), and nasal
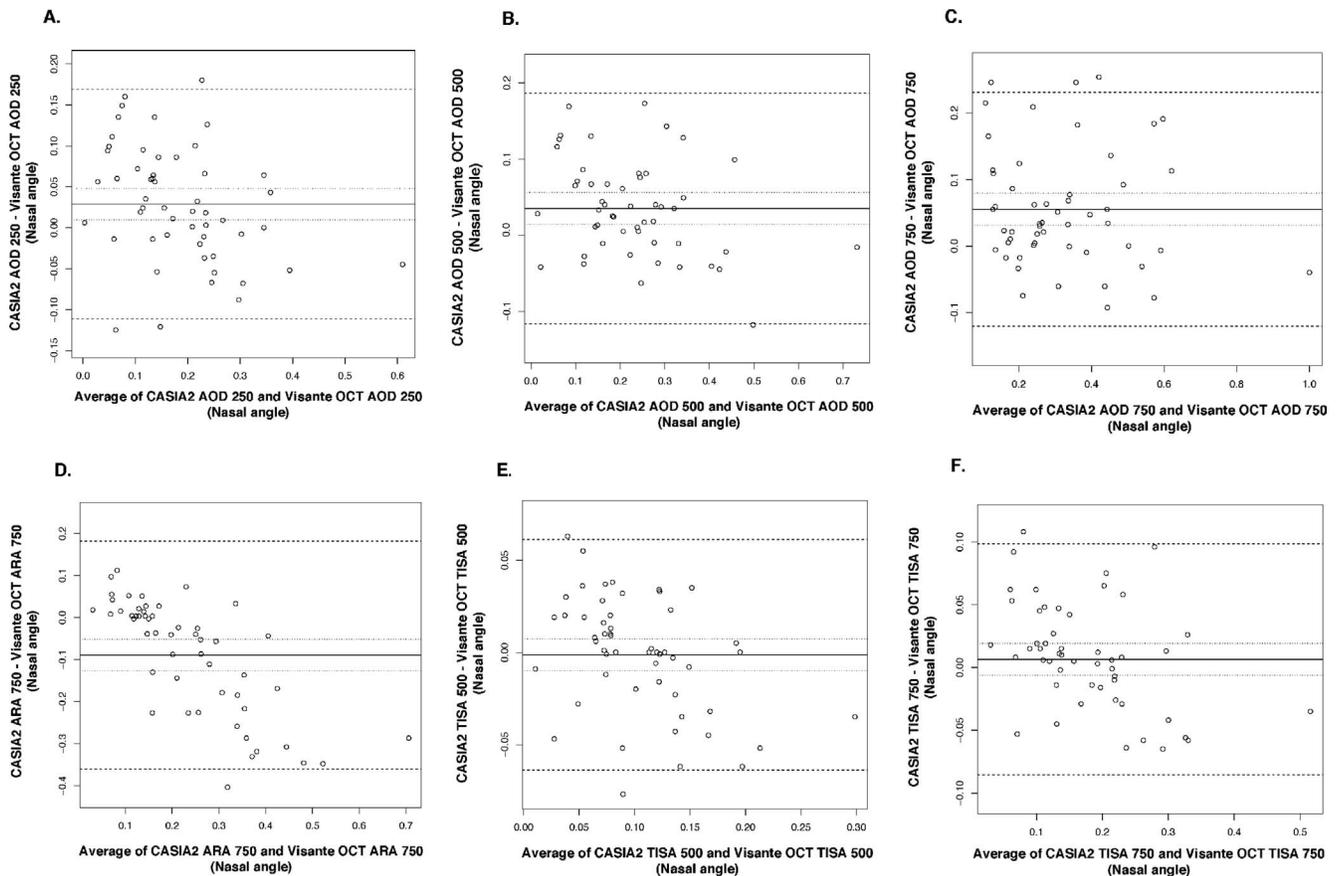
FIGURE 2. Bland-Altman plots for nasal angle parameters. (**A**) AOD250, angle opening distance at 250 μm from SS. (**B**) AOD500, angle opening distance at 500 μm from SS. (**C**) AOD750, angle opening distance at 750 μm from SS. (**D**) ARA750, angle recess area at 750 μm from SS. (**E**) TISA500, trabecular iris space area at 500 μm from SS. (**F**) TISA750, trabecular iris space area at 750 μm from SS.

TISA500 (slope 1.30, 95% CI: 1.12–1.54). The scatterplots with best-fitted or best-fit regression line for ARA750 are shown in Figure 5. We found statistically significant constant biases in nasal AOD250 (intercept −0.09 mm, 95% CI: −0.14 to −0.04 mm); temporal AOD250 (intercept −0.05 mm, 95% CI: −0.09 to −0.01 mm); nasal AOD500 (intercept −0.07 mm, 95% CI: −0.12 to −0.02 mm); nasal AOD750 (intercept −0.08 mm, 95% CI: −0.14 to −0.03 mm); nasal ARA750 (intercept −0.18 mm^2, 95% CI: −0.33 to −0.09 mm^2); temporal ARA750 (intercept −0.19 mm^2, 95% CI: −0.34 to −0.10 mm^2); and nasal TISA750 (intercept −0.05 mm^2, 95% CI: −0.08 to −0.02 mm^2). The negative signs indicate smaller values for Visante OCT compared to CASIA2.

DISCUSSION

Our study evaluated the agreement for six angle parameters, two anterior chamber parameters, and one lens parameter between two dedicated AS-OCT devices—CASIA2 and Visante OCT. Bland-Altman plots demonstrated generally good agreement between the two devices. ICC analysis showed good to excellent correlation in anterior chamber and lens parameters. For the angle parameters, there was good agreement in all angle parameters except ARA750 and temporal AOD500, in which the ICCs fell within the moderate correlation range. In terms of biases, ARA750 possessed significant proportional and constant biases. Regarding the constant bias, the offsets were minimal (−0.09 to −0.05). CASIA2 tended to give greater measurements among parameters that were found to have

constant bias, except for ARA750, where Visante OCT measured larger. There was no evidence of either type of bias among the anterior chamber and lens parameters.

A dedicated AS-OCT is designed to optimize the imaging of anterior segment structures. Compared to posterior segment OCTs, which use wavelengths from 830 to 880 nm, AS-OCT utilizes the wavelength of 1310 nm, which permits high-intensity illumination and increased penetration through the nontransparent tissue such as the sclera. Thus, it allows clear visualization of the angle structures.[16] Currently, there are only a few dedicated AS-OCT models available. The Visante OCT is a first-generation AS-OCT that utilizes time-domain technology. It has a scan speed of 2048 A-scans per second with a transverse resolution of 60 μm and a vertical resolution of 18 μm.[17] Recently, swept-source OCT (SS-OCT), which utilizes a newer time-encoded frequency domain OCT, has been introduced. The CASIA2 incorporates both this and Fourier-domain technology for anterior segment imaging. This newer AS-OCT provides a faster scanning speed of 50,000 A-scans per second, with substantial improvement in the total scanning time of 0.3 to 2.4 seconds.[11] The axial and transverse resolutions are 10 μm or less and 30 μm or less, respectively. A recent study has shown good reproducibility in measuring anterior segment parameters (ICC 0.86–0.99).[18]

Previous published articles have reported the comparison between anterior segment parameters obtained from different OCT modalities. Marion et al.[19] evaluated the agreement of anterior chamber parameters between two spatially encoded Fourier-domain OCTs (FD-OCT), Cirrus and Spectralis OCT, both of which employ the shorter wavelengths (840–870 nm).
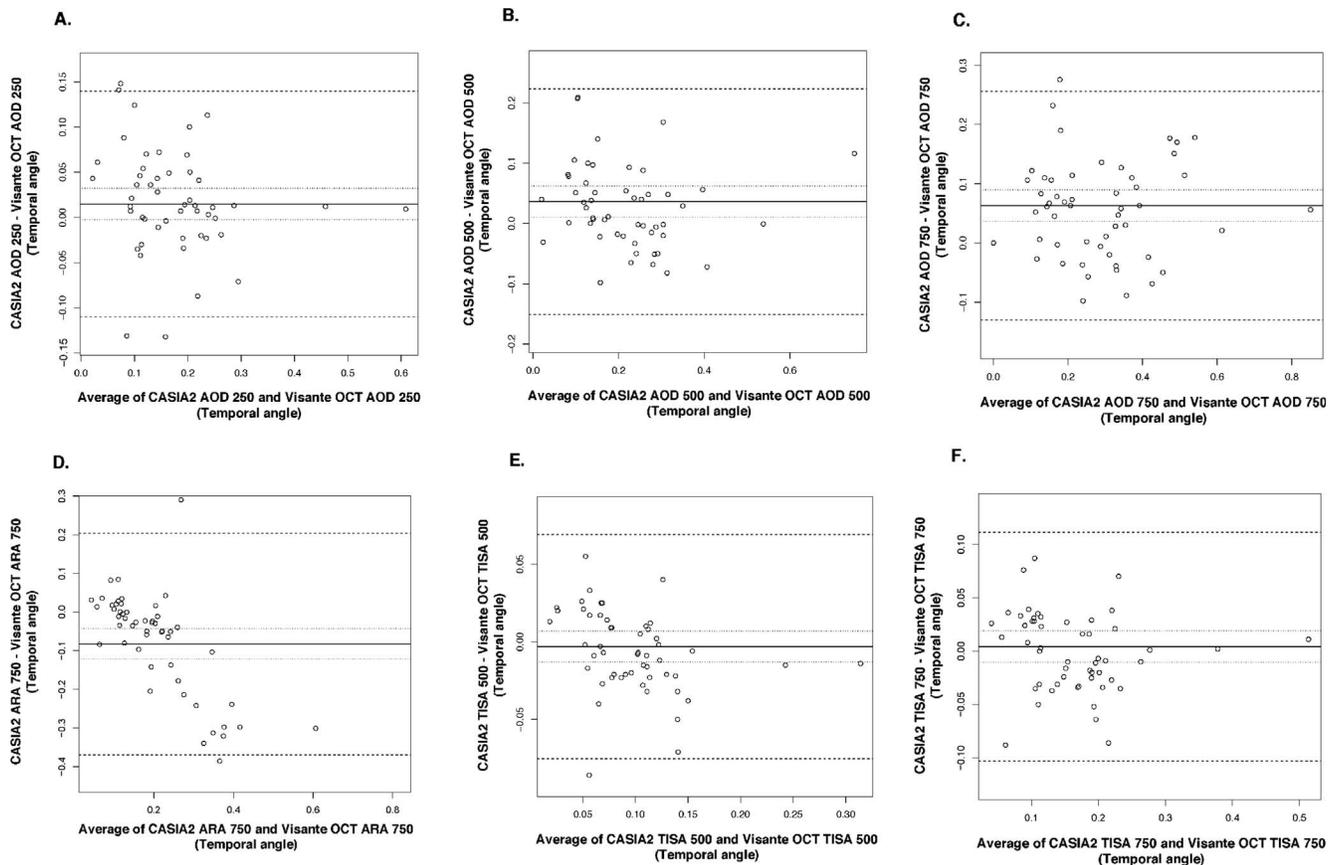
FIGURE 3. Bland-Altman plots for temporal angle parameters. (A) AOD250, angle opening distance at 250 μm from SS. (B) AOD500, angle opening distance at 500 μm from SS. (C) AOD750, angle opening distance at 750 μm from SS. (D) ARA750, angle recess area at 750 μm from SS. (E) TISA500, trabecular iris space area at 500 μm from SS. (F) TISA750, trabecular iris space area at 750 μm from SS.

The measurements obtained from both devices were comparable and could be used interchangeably (ICC > 0.979). However, the parameters in this study were calculated based on identification of Schwalbe's line (SL), not the SS as in our study and most prior studies using AS-OCT. They reported a mean difference of −0.016 mm (LOA −0.125 to 0.092 mm) for SL-AOD (AOD based on identification of SL) and −0.007 mm^2 (LOA −0.056 to 0.043 mm^2) for SL-TISA. Another recent study from Xu et al.[18] found excellent interdevice reproducibility between Spectralis and CASIA2. The reported ICCs were 0.78, 0.78, 0.20, and 0.93 for AOD750, TISA750, ACW, and LV,

respectively. The ICC values from their study were consistent with our findings, except for the ACW, for which their results showed particularly low agreement. The authors speculated that the low ICC in ACW was due to the variability in the scan location. The LOA of their studied parameters also showed wider ranges than our findings (e.g., LOA for TISA750 in Xu et al.,[18] −0.13 to 0.26 vs. −0.006 to 0.019 and −0.010 to 0.019 mm for nasal and temporal, respectively, in the present study). The difference in the wavelengths of the Spectralis OCT2 (880 nm) and CASIA2 (1310 nm) may contribute to the greater span of LOA in their study. For the direct comparison among AS-OCT
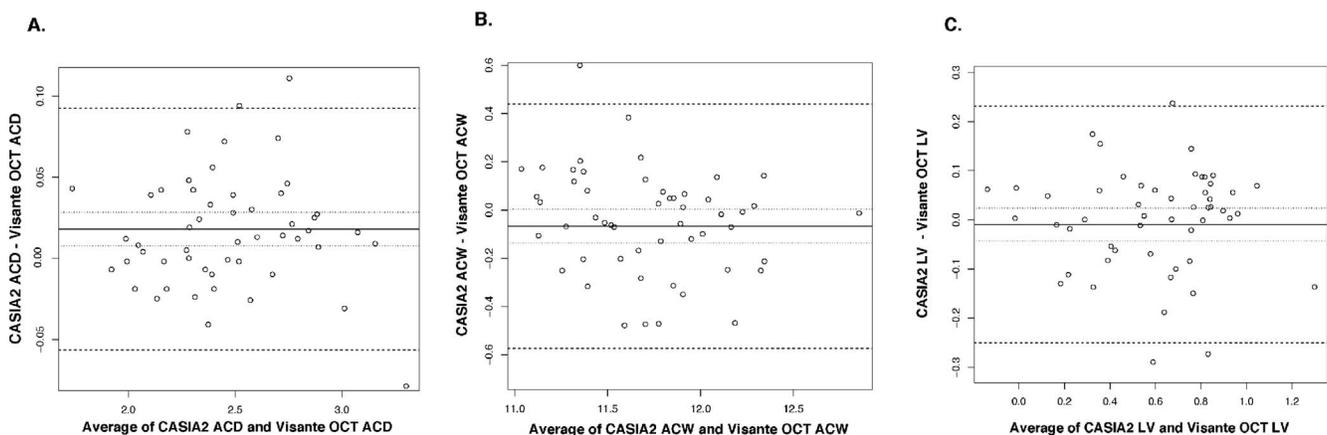

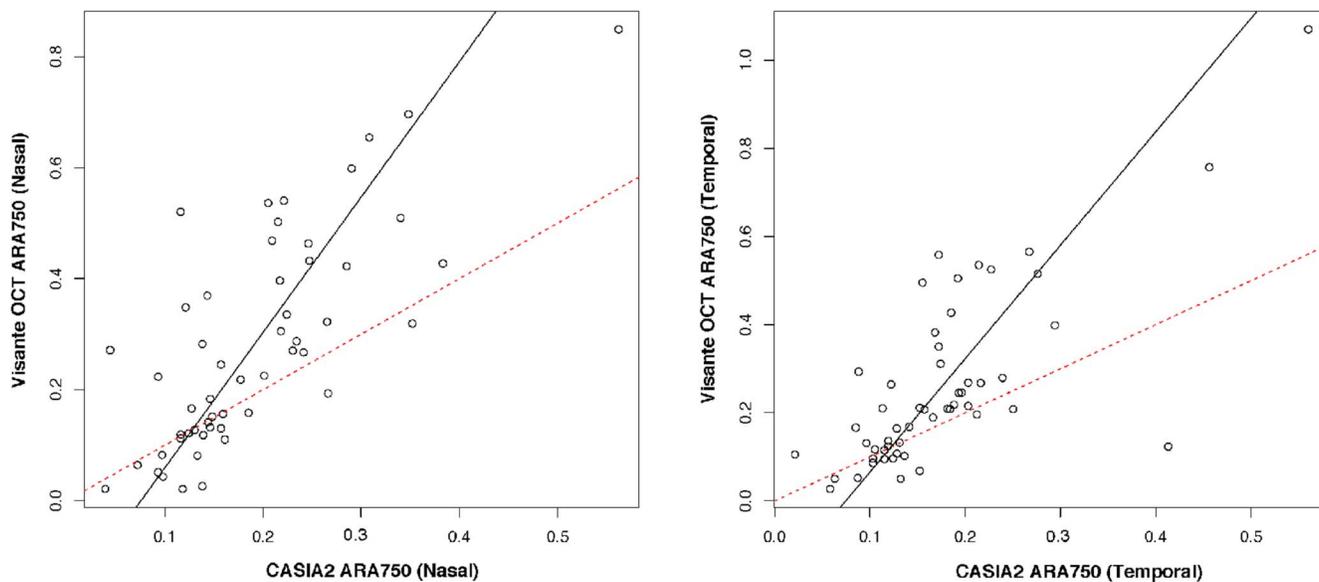FIGURE 4. Bland-Altman plots for anterior chamber and lens parameters. (A) ACD. (B) ACW. (C) LV.

FIGURE 5. Scatterplots of ARA750 from CASIA2 and Visante OCT with regression lines. The regression slope is 2.43 for the nasal angle (*left*) and 2.57 for the temporal angle (*right*), suggesting proportional biases. *Solid line* indicates orthogonal linear regression best-fitted or best-fit line; *dashed line* indicates line with a slope of 1.

devices, Leung et al.[20] compared anterior chamber angle measurements between Visante OCT and slit-lamp OCT. In contrast to the study from Marion et al.[19] and Xu et al.,[18] this study found that there was poor agreement with the wide spans of LOA for the nasal/temporal measurement values, which were 0.437/0.531 mm and 0.174/0.186 mm^2 for AOD500 and TISA500, respectively. Aptel et al.[21] studied the agreement between the Visante OCT and the CASIA SS-1000. The results showed, similar to ours, good agreement between the two devices in AOD500/750 and TISA500/750 and found significant bias in ACD, with greater values in CASIA. This study was conducted with CASIA SS-1000, which was the first-generation swept-source AS-OCT. With updated technology for swept-source imaging, the newer generation CASIA2 improves the image resolution by increasing the scans per line from 512 A-scans in the CASIA SS-1000 to 800 A-scans. Moreover, the images from the Visante OCT in Aptel et al.[21] were assessed with the built-in measurement software, which limits the user to fewer parameters than with the ZAAP software, which allows for the assessment of other notable parameters such as ARA, ACW, and LV.

Based on our data, although most parameters showed good agreement between the two devices, we found significant biases in many angle parameters. The existence of the biases despite the fact that both devices utilize the same wavelengths could be attributable to the differences in the specific OCT technology, the axis for centering the scan, the accommodation induced by internal fixation, and the measurement software algorithm. First, the Visante OCT is a TD-OCT, whereas the CASIA2 is a new generation SS-OCT. Existing data indicate that the difference in OCT technology can result in disparities of the measurement values. Many studies have found discrepancies in various measurements (i.e., corneal thickness, nerve fiber layer thickness, and macular thickness) across the TD-OCT, FD-OCT, and SS-OCT devices.[22-25] It is still unclear whether the discrepancies are a direct result of the differences in the technologies used to acquire images, including the acquiring speed, scanning rate, and image resolution, or in the postcapture data processing, where CASIA2 images are corrected for the effect of refraction at the anterior surface of the cornea as opposed to the Visante OCT

software in which the correction is done in both anterior and posterior surfaces of cornea.[26,27] Second, each machine utilized a different axis for centering the scan. Visante OCT has a manually adjustable centration function. The center of the cross-sectional scan was manually adjusted to achieve images that contain a corneal vertex reflex seen as a bright vertical flare, which indicates alignment with the optical axis. This method is recommended to ensure that angles on both sides are on a meridional plane.[28] As opposed to the Visante OCT, the CASIA2 captures its images in a three-dimensional algorithm. The machine automatically aligns the scan by finding the top point of cornea and captures all its meridional scans using the vertex as the central point. The differences in capture alignment could certainly have an influence on the angle analysis. Third, the internal fixating target could induce some level of accommodation during image acquisition. This near work accommodation may subsequently lead to ciliary body contraction and anterior lens movement.[29] Therefore, the differences in the magnitude of accommodation between the devices may possibly affect the parameter measurements. However, our study showed excellent agreement with no evidence of bias for LV, which would be expected to be affected by accommodation. These results suggest that the influence of accommodation is minimal or approximately the same between both OCT machines. Lastly, the software measurement of the parameters is another factor that could influence the actual values obtained. It is known that the ZAAP software's border detection is based on pixel information and basic edge argument algorithms. The algorithm utilizes data from the extracted 300×600 eight-bit grayscale image in which each pixel is subsequently categorized into tissue or open space by comparing it with a software-calculated threshold value.[30,31] However, the CASIA2 utilizes a proprietary method to carry out segmentation, but there is no public information available regarding the details of their software algorithm.

The considerable proportional bias seen in the nasal and temporal ARA750 showed that the difference between measurement values from the two machines, greater in Visante OCT, became larger as the measurement values increased. This finding is likely to be affected by the location of the angle

recess (AR). Given that no such biases were detected in the TISA measure, which is ARA minus the triangular area peripheral to the line drawn from SS perpendicular to the plane of the inner scleral wall to the opposing iris, the discordance of this triangular area measured by each machine is likely to be a cause of the scaling effect of ARA750 in our findings. The positive slope of the best-fitted or best-fit regression line in ARA750 (the value from the Visante OCT increased approximately 2.5 times with each 1 mm^2 increase in the CASIA2) may represent the tendency for the AR point to be designated at a more peripheral location (more posterior and closer to the scleral wall) in the Visante OCT compared to the CASIA2. One possible explanation is that the better resolution in the CASIA2 can provide better details around the recess area, which is the most crowded part of the angle; thus, in the Visante OCT, the lower pixel density in the small area of the angle recess is prone to be incorrectly detected as an empty space rather than tissue. Hence, the software-generated demarcation of the tissue border can be falsely shifted more toward (or into) the scleral wall in the Visante OCT. Another possibility is that the differences in the measurement software algorithms could lead to the disparities in detecting anatomical landmark tissues. The small area, such as the recess area, could be more sensitive to variations in the software algorithms.

Angle parameters have been proposed as an objective measure to determine angle closure.[8,32] Numerous studies have shown that the Visante OCT has good reliability and reproducibility of the angle parameters.[33,34] Although our analysis showed the good agreement of angle measurement values between CASIA2 and Visante OCT, it is still not recommended that these values be used interchangeably for clinical interpretation. Not only did many angle parameters possess some degree of constant and/or proportional bias, the ranges of the LOA are relatively wide compared to the published cutoffs for detecting narrow angles. For example, Radhakrishnan et al.[35] evaluated angle parameters with Visante OCT and proposed the AOD500 cutoff of 0.191 mm for occludable angle, and our data show the LOA of nasal AOD500 to be −0.117 to 0.187 mm, in which the upper limit (0.187) is almost equal to the cutoff. Moreover, among most of the parameters with significant biases, CASIA2 tended to provide higher measurements and thus could lead to a tendency toward assessment of an open angle in CASIA2 compared to Visante OCT, perhaps including when clinicians assess images subjectively. In contrast, ARA750 that was documented for proportional biases had greater value in the Visante. Using a temporal ARA750 cutoff of 0.191 mm^2 as proposed by Narayanaswamy et al.,[8] an example case where the measurement is 0.174 mm^2 by CASIA2 and 0.311 mm^2 by Visante OCT would be classified as closed angle with CASIA2 but open angle with Visante OCT. Our results, taken together with the published data, highlight that the use of the cutoffs may need to be device specific. When comparing across the different OCT devices, TISA tends to have the smallest mean difference and good to excellent ICC, whereas parameters related to the recess point (i.e., ARA, trabecular iris angle, SS angle) tend to be disparate among devices.[18–21]

The strength of our study is that we used a single OCT operator and a single image grader, which could help to minimize the variability of the image acquisition and the parameter measurements. The nasal and temporal angles were analyzed separately for best direct comparison. In addition, the images were graded in random sequence to reduce the potential bias. However, our study has some limitations. First, approximately one third of our study samples were angle closure. This group is known to have smaller values of angle parameters; therefore, the values might not be equally distributed to the whole range of angle widths. Nevertheless,

since most of the patients who require AS-OCT scanning for making therapeutic decisions have narrow angles, our data may represent the distribution in a practical clinical setting. Second, we focused only on the agreement in the measurement values and did not evaluate the diagnostic ability in detecting angle closure disease. In addition, only images at the horizontal scans were included for analysis. Although the CASIA2 is able to obtain up to 128 radial cross-sectional images covering 360 degrees in a single capture, we used only the horizontal scan for direct comparison with the standard horizontal scan of the Visante OCT. Future studies may also compare other meridians, although care must be taken to avoid pressure against the eye when holding the eyelids to access the vertical scans. Last, the current limited use of AS-OCT by clinicians may constrain the utility of our data in current clinical practice. In the future, however, as many researchers and device companies develop automated software to distinguish narrow/closed angles using measurement parameters, the use and interpretation of AS-OCT parameters may become simpler and more user-friendly for clinicians.

In conclusion, the CASIA2 and Visante OCTs had generally good agreement, especially for anterior chamber and lens parameters. However, there was evidence of proportional and constant biases for most angle parameters. Among those parameters with constant biases, CASIA2 tends to give greater numbers. The proportional biases were most prominent in the ARA750. It is not recommended that the measurement values be used interchangeably across the devices.

References

1. Quigley HA, Broman AT. The number of people with glaucoma worldwide in 2010 and 2020. *Br J Ophthalmol.* 2006;90:262–267.

2. Tham YC, Li X, Wong TY, Quigley HA, Aung T, Cheng CY. Global prevalence of glaucoma and projections of glaucoma burden through 2040: a systematic review and meta-analysis. *Ophthalmology.* 2014;121:2081–2090.

3. Quigley HA, Broman AT. The number of people with glaucoma worldwide in 2010 and 2020. *Br J Ophthalmol.* 2006;90:262–267.

4. Moghimi S, Vahedian Z, Fakhraie G, et al. Ocular biometry in the subtypes of angle closure: an anterior segment optical coherence tomography study. *Am J Ophthalmol.* 2013;155: 664–673.e1.

5. Smith SD, Singh K, Lin SC, et al. Evaluation of the anterior chamber angle in glaucoma: a report by the American Academy of Ophthalmology. *Ophthalmology.* 2013;120: 1985–1997.

6. Pekmezci M, Porco TC, Lin SC. Anterior segment optical coherence tomography as a screening tool for the assessment of the anterior segment angle. *Ophthalmic Surg Lasers Imaging.* 2009;40:389–398.

7. Nolan WP, See JL, Chew PT, et al. Detection of primary angle closure using anterior segment optical coherence tomography in Asian eyes. *Ophthalmology.* 2007;114:33–39.

8. Narayanaswamy A, Sakata LM, He MG, et al. Diagnostic performance of anterior chamber angle measurements for detecting eyes with narrow angles: an anterior segment OCT study. *Arch Ophthalmol*. 2010;128:1321–1327.

9. Wu RY, Nongpiur ME, He MG, et al. Association of narrow angles with anterior chamber area and volume measured with anterior-segment optical coherence tomography. *Arch Ophthalmol*. 2011;129:569–574.

10. Wang B, Sakata LM, Friedman DS, et al. Quantitative iris parameters and association with narrow angles. *Ophthalmology*. 2010;117:11–17.

11. Tomey Corporation. Fourier domain OCT CASIA2. Available at: http://tomey.de/images/product_flyer/CASIA2_br_w.pdf. Accessed November 21, 2017.

12. Sakata LM, Wong TT, Wong HT, et al. Comparison of Visante and slit-lamp anterior segment optical coherence tomography in imaging the anterior chamber angle. *Eye (Lond)*. 2010;24: 578–587.

13. Seager FE, Wang J, Arora KS, Quigley HA. The effect of scleral spur identification methods on structural measurements by anterior segment optical coherence tomography. *J Glaucoma*. 2014;23:e29–38.

14. Lin S, Huang J-Y. Clinical application of anterior segment optical coherence tomography for angle-closure related disease. *Taiwan J Ophthalmol*. 2012;2:77–80.

15. Koo TK, Li MY. A guideline of selecting and reporting intraclass correlation coefficients for reliability research. *J Chiropr Med*. 2016;15:155–163.

16. Radhakrishnan S, Yarovoy D. Development in anterior segment imaging for glaucoma. *Curr Opin Ophthalmol*. 2014;25:98–103.

17. Maram J, Sorbara L, Simpson T. Accuracy of Visante and Zeiss-Humphrey optical coherence tomographers and their cross calibration with optical pachymetry and physical references. *J Optom*. 2011;4:147–155.

18. Xu BY, Mai DD, Penteado RC, Saunders L, Weinreb RN. Reproducibility and agreement of anterior segment parameter measurements obtained using the CASIA2 and Spectralis OCT2 optical coherence tomography devices. *J Glaucoma*. 2017;26:974–979.

19. Marion KM, Maram J, Pan X, et al. Reproducibility and agreement between 2 spectral domain optical coherence tomography devices for anterior chamber angle measurements. *J Glaucoma*. 2015;24:642–646.

20. Leung CK, Li H, Weinreb RN, et al. Anterior chamber angle measurement with anterior segment optical coherence tomography: a comparison between slit lamp OCT and Visante OCT. *Invest Ophthalmol Vis Sci*. 2008;49:3469–3474.

21. Aptel F, Chiquet C, Gimbert A, et al. Anterior segment biometry using spectral-domain optical coherence tomography. *J Refract Surg*. 2014;30:354–360.

22. Ha A, Lee SH, Lee EJ, Kim TW. Retinal nerve fiber layer thickness measurement comparison using spectral domain and swept source optical coherence tomography. *Korean J Ophthalmol*. 2016;30:140–147.

23. Sung KR, Kim JS, Wollstein G, Folio L, Kook MS, Schuman JS. Imaging of the retinal nerve fibre layer with spectral domain optical coherence tomography for glaucoma diagnosis. *Br J Ophthalmol*. 2011;95:909–914.

24. Li H, Leung CK, Wong L, et al. Comparative study of central corneal thickness measurement with slit-lamp optical coherence tomography and Visante optical coherence tomography. *Ophthalmology*. 2008;115:796–801.e2.

25. Ibrahim MA, Sepah YJ, Symons RC, et al. Spectral- and time-domain optical coherence tomography measurements of macular thickness in normal eyes and in eyes with diabetic macular edema. *Eye (Lond)*. 2012;26:454–462.

26. Schallhorn JM, Tang M, Li Y, Song JC, Huang D. Optical coherence tomography of clear corneal incisions for cataract surgery. *J Cataract Refract Surg*. 2008;34:1561–1565.

27. Sakata LM. Anterior-segment imaging for anterior chamber angle assessment. *e-Oftalmo.CBO: Rev Dig Oftalmol*. 2016;2: 1–14.

28. Steinert RF, Huang D. *Anterior Segment Optical Coherence Tomography*. Thorofare, NJ: SLACK; 2008.

29. Goldberg DB. Computer-animated model of accommodation and theory of reciprocal zonular action. *Clin Ophthalmol*. 2011;5:1559–1566.

30. Ang M, Chong W, Huang H, et al. Comparison of anterior segment optical tomography parameters measured using a semi-automatic software to standard clinical instruments. *PLoS One*. 2013;8:e65559.

31. Console JW, Sakata LM, Aung T, Friedman DS, He M. Quantitative analysis of anterior segment optical coherence tomography images: the Zhongshan Angle Assessment Program. *Br J Ophthalmol*. 2008;92:1612–1616.

32. Lavanya R, Foster PJ, Sakata LM, et al. Screening for narrow angles in the Singapore population: evaluation of new noncontact screening methods. *Ophthalmology*. 2008;115: 1720–1727.e2.

33. Radhakrishnan S, See J, Smith SD, et al. Reproducibility of anterior chamber angle measurements obtained with anterior segment optical coherence tomography. *Invest Ophthalmol Vis Sci*. 2007;48:3683–3688.

34. Li H, Leung CK, Cheung CY, et al. Repeatability and reproducibility of anterior chamber angle measurement with anterior segment optical coherence tomography. *Br J Ophthalmol*. 2007;91:1490–1492.

35. Radhakrishnan S, Goldsmith J, Huang D, et al. Comparison of optical coherence tomography and ultrasound biomicroscopy for detection of narrow anterior chamber angles. *Arch Ophthalmol*. 2005;123:1053–1059.

Author/s:
Chansangpetch, S;Nguyen, A;Mora, M;Badr, M;He, M;Porco, TC;Lin, SC

Title:
Agreement of Anterior Segment Parameters Obtained From Swept-Source Fourier-Domain and Time-Domain Anterior Segment Optical Coherence Tomography

Date:
2018-03-01